Crack edge collocation for the direct computation of stress intensity factors using the displacement discontinuity method

J.A.L. Napier*

The numerical solution of problems relating to crack fracture and failure can be accomplished using the displacement discontinuity boundary element method. This paper presents an extension to the normal formulation of this method to enable stress intensity factors to be solved directly at the crack edges. This is achieved by employing an enhanced edge collocation procedure. The limiting interpretation of the governing integral equations is discussed and two simple examples are presented to illustrate the application of the method.

Introduction

Two well-established methods for the numerical analysis of boundary value problems in potential theory and elasticity are the finite element method (FEM) and the boundary element method (BEM). Relying on the existence of fundamental solutions, the BEM is usually restricted to problems with homogeneous material properties. Nevertheless, this approach may often be the method of first choice when considering the analysis of problems that are dominated by the behaviour of significant boundary or internal surfaces. A particular example is the treatment of tabular mining problems, introduced in South Africa by Salamon,[1] Starfield and Crouch,[2] and Crouch.[3] This technique, now termed the displacement discontinuity method (DDM), has been employed also in the solution of problems of earthquake dynamics[4,5] and in general crack propagation studies.[6]

The DDM requires the solution of a singular integral equation that can, in the case of a flat crack surface, be treated effectively by dividing the surface into a number of uniform square elements.[1,7] In the simplest case, it is assumed that the crack slip or opening displacement is constant within each element and that the element 'influence', in terms of induced stress values, can be derived analytically at the centres of all the surrounding elements to form a matrix approximation to the integral equation. In problems relating to deep-level gold mining, where reef excavations typically extend over areas of several square kilometres, the derived influence matrix may be extremely large (of the order of 50 000 or more) requiring special numerical treatment. An innovative, and then novel, use of the Fast Fourier technique was proposed by Starfield (pers. comm.) for the solution of these problems and its viability was demonstrated by Stuart.[8]

A central issue in the use of the DDM is the evaluation of the boundary integral relationship at any given point on the crack surface.[9] Owing to the nature of the singular kernel in the integral equation, this requires special care in any numerical treatment. Most of the early applications of the DDM[7-10] consequently employed collocation methods, where the limiting behaviour is evaluated at a point internal to the element surface (typically at the element centre for constant, square elements). Recent proposals[11] have suggested that this collocation point can be located at a common vertex of adjoining elements. This paper discusses the restrictions that are associated with this procedure and then proposes the novel concept of placing collocation points on the edge of the crack surface. In this case the stress intensity factor is evaluated directly, rather than being inferred from the value of the adjacent crack opening displacement. This has the advantage of providing immediately one of the key parameters of interest in fracture mechanics and in the analysis of crack growth problems. In the context of tabular mine design, this approach may be used for the direct evaluation of the energy release rate along the edges of mine excavations.

*CSIR Division of Mining Technology, P.O. Box 91230, Auckland Park 2006, Johannesburg, South Africa. E-mail: jnapier@csir.co.za

Boundary integral equation singularities

The components of the stress tensor induced at point P by the displacement discontinuity vector $D_i(Q)$ defined at the points Q of a crack surface ∂B are given by the expression

$$\tau_{kl}(P) = \int_{\partial B} \Gamma_{ijkl}(P,Q) D_i(Q) n_j(Q) dS_Q \,, \qquad (1)$$

where $D_i(Q) = u_i^+(Q) - u_i^-(Q)$ and where $u_i^+(Q)$ and $u_i^-(Q)$ are the components of the displacement vector on the 'positive' and 'negative' sides of the surface with respect to the defined positive normal $n_i(Q)$. dS_Q is the elementary surface area at point Q. The influence tensor Γ_{ijkl} depends on the relative distance r between points P and Q as well as the direction cosines γ_i of point P relative to point Q.[3] Repeated indices in the integrand in Equation (1) are assumed to be summed. Problems in elastodynamics can be reduced to a similar, but functionally more complex form.[4]

Consider the simplified case of a single, flat crack lying in the plane $z = 0$ and subjected to a far field stress that acts perpendicularly to the fracture surface. The explicit form of Equation (1) for the normal stress component, τ_{zz}, induced by the crack in an isotropic elastic medium, is given by

$$\tau_{zz}(P) = C_e \iint_{\partial B} \frac{1}{r^3} [1 + 6\gamma_z^2 - 15\gamma_z^4] D_z(\xi,\eta) d\xi d\eta \,, \qquad (2)$$

where point P has coordinates (x,y,z), $\gamma_z = z/r$, $r^2 = (x-\xi) + (y-\eta)^2 + z^2$ and $D_z(\xi,\eta)$ is the normal component of the displacement discontinuity vector at point $Q(\xi,\eta)$. The constant C_e depends on the elastic properties of the medium and is given by

$$C_e = G/4\pi(1-\nu) \,, \qquad (3)$$

where G is the shear modulus and ν is Poisson's ratio.

Care must be taken in evaluating Equation (2) when the field point P tends to the surface ∂B (that is when $z \to 0$). The analysis of this limit can be simplified by expressing the integrand in Equation (2) in polar coordinates. In particular, by setting $x - \xi = \rho \cos\theta$ and $y - \eta = \rho \sin\theta$, Equation (2) can be written in the form

$$\tau_{zz}(P_o, z) = C_e \int \Big\{ \int_0^{R(\theta)} D_z(\rho,\theta)(\rho^2 + z^2)^{-3/2} [1 + 6\gamma_z^2 - 15\gamma_z^4] \rho d\rho \Big\} d\theta \,, \qquad (4)$$

where P_o designates the expansion point (x,y), $r^2 = \rho^2 + z^2$ and $R(\theta)$ represents the distance from the expansion point P_o to the crack boundary. The outer integral, with respect to θ, is considered to imply a complete circuit around the crack boundary. In the special case where D_z is a simple polynomial function of $x-\xi$ and $y-\eta$ it is possible to express D_z in the form of a series

$$D_z(\rho,\theta) = c_o + \sum_{k=1}^{n} f_k(\theta)\rho^k, \tag{5}$$

where c_o is a constant and $f_k(\theta)$ are trigonometric polynomials in $\sin\theta$ and $\cos\theta$. The upper limit of the sum, n, defines the order of the expansion. The inner integral in Equation (4) can be evaluated analytically in this case and the limiting behaviour as $z \to 0$ can be determined. Carrying out the inner integration, Equation (4) may be written in the form

$$\tau_{zz}(P_o, z) = \int \sum_{k=0}^{n} f_k(\theta)[F_k(R) - F_k(0)]d\theta \tag{6}$$

where,

$$F_k(\rho) = \int \frac{\rho^{k+1}}{r^3}\left[1 + 6z^2/r^2 - 15z^4/r^4\right]d\rho \tag{7}$$

and it is assumed that $f_0(\theta) = c_o$. The limiting case $z \to 0$ is then determined by the behaviour of the integrals $F_k(\rho)$ as $z \to 0$. Considering the first three terms of the series in Equation (6), it may be shown that

$$F_0(\rho) = -\rho^2(\rho^2 + 4z^2)/(\rho^2 + z^2)^{5/2}, \tag{8}$$

$$F_1(\rho) = -\rho(\rho^4 + 5\rho^2 z^2 + z^4)/(\rho^2 + z^2)^{5/2} + \ln\left[\rho + \sqrt{(\rho^2 + z^2)}\right], \tag{9}$$

$$F_2(\rho) = \rho^4(\rho^2 - 2z^2)/(\rho^2 + z^2)^{5/2}. \tag{10}$$

Examination of Equations (8), (9) and (10) reveals that, for $\rho > 0$, $F_k(\rho)$ remains finite when $z \to 0$. When $\rho \to 0$, both $F_0(\rho) \to 0$ and $F_2(\rho) \to 0$ when z is not zero. In this case the zero terms, $F_0(0)$ and $F_2(0)$, in the integrand of Equation (6) do not contribute to the value of the induced stress $\tau_{zz}(P_o,z)$ and are assumed also to give no contribution when $z \to 0$. However, when $\rho = 0$,

$$F_1(0) = \ln(\sqrt{z^2}) \tag{11}$$

and the integrand in Equation (6) becomes unbounded as $z \to 0$. For a function $D_z(\rho,\theta)$ possessing a smooth tangent at $\rho = 0$, the expansion function $f_1(\theta)$ must assume the form

$$f_1(\theta) = \alpha_1 \cos\theta + \beta_1 \sin\theta, \tag{12}$$

where α_1 and β_1 are constants defining the local tangent slope. The contributions to the induced stress from the F_1 terms in Equation (6) then become

$$\tau_{zz}^{(1)} = \int (\alpha_1 \cos\theta + \beta_1 \sin\theta)\left[F_1(R(\theta)) - \ln\sqrt{z^2}\right]d\theta \tag{13}$$

and it can be seen that the potentially singular terms involving $\sqrt{z^2}$ vanish when the integral is evaluated around the perimeter of the crack.

In summary, it is therefore apparent that if the crack opening displacement function $D_z(\rho,\theta)$ possesses a locally smooth tangent at a given point P_o on the crack surface, then the stress induced at the point will be bounded. This provides, as well, a sufficient condition for the evaluation of the traction vector at the common vertex, P_o, of a set of adjoining elements as shown in Fig. 1. This places some constraints on the implementation of a 'node-centric' collocation scheme such as the method proposed by Vijayakumar *et al.*[11] This condition will not be satisfied if each element at the vertex has a different tangent plane at the common point. This would arise, for example, if it were assumed that the discontinuity variation was linear within each of the adjoining elements. However, if a numerical procedure is devised in which the uniform tangent condition is ensured at each common vertex, then traction boundary conditions can be evaluated at each vertex by adjustment of the crack displacement discontinuity components.

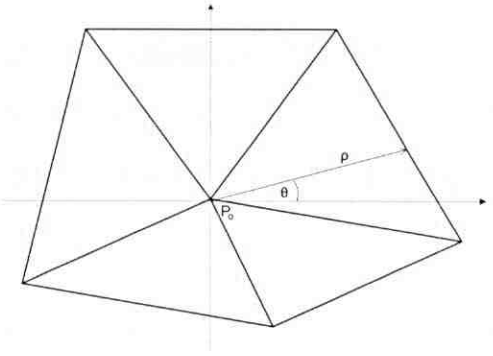

Fig. 1. Polar integration about a common vertex P_o shared by five triangular displacement discontinuity elements.

Edge collocation procedure

Imposing the condition of a uniform tangent plane for the displacement discontinuity components at point P_o of the crack surface and letting $z \to 0$ in Equations (8)–(10), yields the following values for the functions $F_k(R)$:

$$\lim_{z\to 0} F_0(R) = -\frac{1}{R}, \tag{14}$$

$$\lim_{z\to 0} F_1(R) = -1 + \ln 2 + \ln R, \tag{15}$$

$$\lim_{z\to 0} F_2(R) = R. \tag{16}$$

If the expression for $F_1(R)$, given by Equation (15), is substituted into Equation (13), it is apparent that the constant $-1 + \ln 2$ does not contribute to the value of $\tau_{zz}^{(1)}$ when the integral is evaluated. From these results, it appears therefore that when $z \to 0$, Equation (4) can be written formally as

$$\tau_{zz}(P_o) = C_e \int_0 \int^{R(\theta)} \frac{D_z(\rho,\theta)}{\rho^2} d\rho d\theta \tag{17}$$

and the inner integral in Equation (17) may be evaluated directly once the functional form of the crack opening displacement $D_z(\rho,\theta)$ is assigned. This is equivalent to interpreting the inner integral in Equation (17) in terms of Hadamard's finite part of a divergent integral.[12] This effectively allows the immediate derivation of Equations (14)–(16) by evaluating the inner integral in Equation (17) formally and ignoring the lower limit of integration, $\rho = 0$. [The constant $-1 + \ln 2$ will not appear in Equation (15) in this case, but may be omitted as it will not contribute to the outer integral in Equation (17)]. Consequently, provided the smooth tangent condition is satisfied, it seems feasible to choose the collocation point P_o at any position within the crack surface, including the limiting case when this point tends to the edge of the crack from within the crack region.

To motivate this suggestion further, consider the analysis of a parallel-sided crack located in the region $0 \le y \le H$ of the x–y

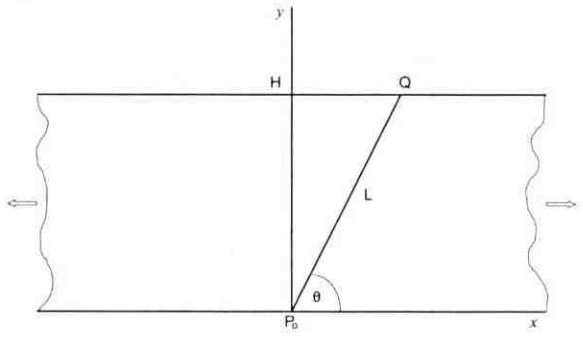

Fig. 2. Parallel-sided crack defined in the region $0 \le y \le H$ of the x–y plane.

plane as shown in Fig. 2. Suppose that the distance between the collocation point P_0 and a point Q located on the opposite edge of the crack is equal to L and that the line P_0Q is inclined at an angle θ to the x-axis as shown in Fig. 2. Hence,

$$L(\theta) = H / \sin\theta \; ; \; 0 < \theta < \pi \; . \tag{18}$$

Furthermore, suppose that the crack opening displacement along the line P_0Q is given by the function

$$D_z(\rho,\theta) = [\rho(L-\rho)]^{1/2}(\alpha_1 + \alpha_2\rho) \; . \tag{19}$$

Also, suppose that near the crack edges, $y = 0$ and $y = H$, the crack opening displacement can be expressed as follows.

$$\lim_{\varepsilon\to 0} D_z(\varepsilon,\theta) = k_1\sqrt{\varepsilon} \; , \; y = 0 \tag{20}$$

$$\lim_{\varepsilon\to 0} D_z(L-\varepsilon,\theta) = k_2\sqrt{\varepsilon} \; , \; y = H \; . \tag{21}$$

Using Equations (20) and (21), Equation (19) may be expressed in terms of 'shape' functions $\psi_1(\rho)$ and $\psi_2(\rho)$, for $0 \le \rho \le L$, in the form

$$D_z(\rho,6) = k_1\psi_1 + k_2\psi_2 \; , \tag{22}$$

where

$$\psi_1(\rho) = \frac{1}{\sqrt{L}}[\rho(L-\rho)]^{1/2}(1-\rho/L) \; , \tag{23}$$

$$\psi_2(\rho) = \frac{1}{\sqrt{L}}[\rho(L-\rho)]^{1/2}(\rho/L) \tag{24}$$

and $L(\theta)$ is given by Equation (18).

Employing Equations (22)–(24), Equation (17) can be evaluated in terms of the following integrals:

$$A_1(\rho) = \int \frac{[\rho(L-\rho)]^{1/2}}{\rho}\,d\rho = [\rho(L-\rho)]^{1/2} + L\tan^{-1}\sqrt{\frac{\rho}{L-\rho}} \; , \tag{25}$$

$$A_2(\rho) = \int \frac{[\rho(L-\rho)]^{1/2}}{\rho^2}\,d\rho = -2\sqrt{\frac{L-\rho}{\rho}} - 2\tan^{-1}\sqrt{\frac{\rho}{L-\rho}} \; . \tag{26}$$

It can be seen from Equation (26) that substitution of the lower limit $\rho = 0$ results in a singular expression for A_2. If it is assumed that Hadamard's finite part interpretation, as motivated in the derivation of Equations (14)–(16), can be applied to Equation (26) then the value for A_2 is evaluated by substituting the upper limit $\rho = L$ into Equation (26) and the lower limit, $\rho = 0$, is ignored. Hence,

$$A_1(L) = \pi L / 2 \; , \tag{27}$$

$$A_2(L) = -\pi \; . \tag{28}$$

Using these values and employing Equations (22), (23) and (24), allows Equation (17) to be reduced to the form

$$T(P_o) = -C_e\int_0^{\pi}\left[\frac{3\pi k_1(\theta)}{2\sqrt{L(\theta)}} - \frac{\pi k_2(\theta)}{2\sqrt{L(\theta)}}\right]d\theta \; , \tag{29}$$

where $T(P_0)$ designates the normal traction component relative to the crack surface and C_e is given by Equation (3). For the parallel-sided crack geometry shown in Fig. 2, it is assumed that the crack is opened by a linearly varying internal pressure given by T_1 on $y = 0$ and T_2 on $y = H$. Hence, T varies across the width of the crack according to

$$T(y) = T_1 + (T_2 - T_1)y/H \; ; \; 0 \le y \le H \; . \tag{30}$$

In this case, the crack edge opening coefficients k_1 and k_2 are uniform along each edge. Along the particular direction P_0Q, k_1 and k_2 are given by

$$k_1(\theta) = k_1^0\sqrt{\sin\theta} \; , \tag{31}$$

$$k_2(\theta) = k_2^0\sqrt{\sin\theta} \; , \tag{32}$$

where k_i^0 is used to denote the value of $k_i(\theta)$ when $\theta = 0$, $i = 1,2$. Employing Equations (31) and (32), together with Equation (18), enables Equation (29) to be evaluated at each edge of the crack. This yields two simultaneous equations for the tractions T_1 and T_2 in the form

$$T_1 = \frac{-G}{4(1-\nu)\sqrt{H}}\left[3k_1^0 - k_2^0\right], \tag{33}$$

$$T_2 = \frac{-G}{4(1-\nu)\sqrt{H}}\left[3k_2^0 - k_1^0\right]. \tag{34}$$

If $T_1 = 0$ and $T_2 = -2\,\bar{p}$, where $\bar{p}$ is the average pressure in the crack, Equations (33) and (34) can be solved to give

$$k_1^0 = (1-\nu)\bar{p}\sqrt{H}/G \; , \tag{35}$$

$$k_2^0 = 3(1-\nu)\bar{p}\sqrt{H}/G \; . \tag{36}$$

Assuming that the crack front is locally smooth and in a state of plane strain, the stress intensity factor K_I can be inferred from the crack edge coefficient k, using standard crack tip expansions (see, for example, Cherepanov[13]), to be

$$K_I = \frac{\sqrt{2\pi}G}{4(1-\nu)}k \; . \tag{37}$$

Substituting the values of k_1^0 and k_2^0 given by Equations (35) and (36) into Equation (37), yields

$$K_{I1} = \sqrt{2\pi H}\,\bar{p}/4 \; ; \; K_{I2} = 3K_{I1} \; , \tag{38}$$

which agrees with the analytic expressions given by Cherepanov.[13] It must be noted that these results depend directly on the choice of the shape functions defined by Equations (23) and (24). In the present case, these represent the best possible choice corresponding to the exact solution for the parallel-sided crack with a linearly varying internal pressure. However, the main consideration dictating this choice is to ensure that the characteristic limiting behaviour defined by Equations (20) and (21) is represented.

Flat elliptical crack

A second demonstration of the proposed edge collocation scheme is the case of a flat, elliptical crack, depicted in Fig. 3. The coordinates of points on the perimeter of the crack are defined

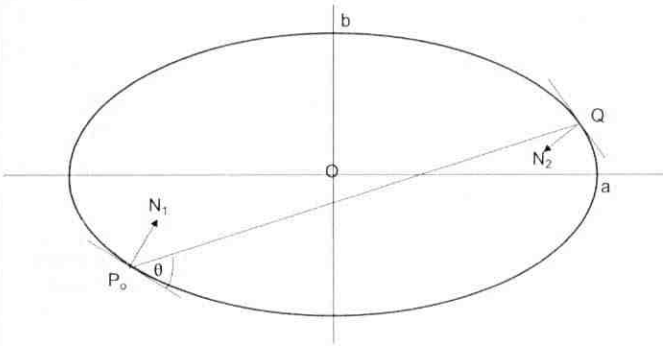

Fig. 3. Flat elliptical crack with chord P_oQ and local inward normal vectors N_1 and N_2 at points P_o and Q respectively.

parametrically in terms of the angular variable β by $x = a\cos\beta$, $y = b\sin\beta$, where $2a$ and $2b$ are the lengths of the major and minor axes, respectively. It may again be assumed that the crack opening displacement across any chord P_oQ (see Fig. 3) is given by Equation (19). Employing Equation (29), it is apparent that at each point on the perimeter of the crack, the traction just inside the crack edge must obey the equation

$$T(P_o) = \frac{-G}{8(1-\nu)}\int_0^{\pi}\left[\frac{3k_1(\theta)}{\sqrt{L(\theta)}} - \frac{k_2(\theta)}{\sqrt{L(\theta)}}\right]d\theta. \qquad (39)$$

The function $k_2(\theta)$ is implied by the specific orientation of the chord P_oQ and the inward normals to the crack front at points P_o and Q, respectively. Some care must be taken in the evaluation of the integrand near the limits $\theta = 0$ and $\theta = \pi$. In these cases, the limiting behaviour can be determined by approximating the crack edge locally at point P_o by a circular arc whose curvature, κ, matches the curvature of the elliptical crack boundary. The limiting chord length L is then given by

$$\lim_{\theta\to 0} L(\theta) = \frac{2}{\kappa}\sin\theta, \qquad (40)$$

and the local radius of curvature is equal to $1/\kappa$. Since $k_1(\theta) = k_1(0)\sqrt{\sin\theta}$, and $k_2(\theta) \to k_1(\theta)$ as $\theta \to 0$, the integrand in Equation (39) tends to $\sqrt{2\kappa}k_1(0)$ as $\theta \to 0$. (In the case of the parallel-sided crack treated previously, $\kappa = 0$.)

Applying Equation (39) to a series of points P_i around the perimeter of the elliptical crack, yields a set of equations in terms of the unknown edge expansion coefficients $k(P_i)$ at each boundary point. These may be transformed to the stress intensity factor using Equation (37). In the case of a uniformly loaded elliptical crack, the stress intensity factor along the crack perimeter can be expressed in terms of the angular parameter β in the form[13]

$$K_I(\beta) = \frac{\bar{p}\sqrt{\pi b}}{E(m)}\left[\sin^2\beta + (b/a)^2\cos^2\beta\right]^{1/4}, \qquad (41)$$

where $2a$ and $2b$ are the major and minor axis lengths, as defined previously, and $\bar{p}$ is the applied internal pressure. $E(m)$ is the complete elliptic integral of the second kind defined by

$$E(m) = \int_0^{\pi/2}\sqrt{1-m^2\sin^2\phi}\,d\phi;\ m^2 = 1-b^2/a^2. \qquad (42)$$

As a specific example, an elliptical crack was considered with dimensions a = 20 m, b = 5 m and $\bar{p}$ = 100 MPa. The elastic constants were chosen as G = 29167 MPa and υ = 0.2. The edge collocation points were chosen to have a nominal spacing of 1 m along the crack perimeter, resulting in a total of 86 boundary points. The local edge curvature at each point was estimated by computing the radius of the circle passing through each point

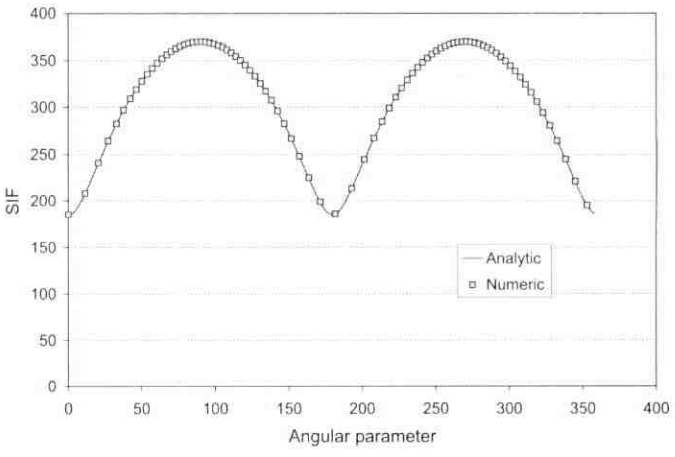

Fig. 4. Comparison of the analytic distribution of the stress intensity factor around the perimeter of a 4:1 elliptical crack to the numerical solution computed using the proposed edge collocation procedure.

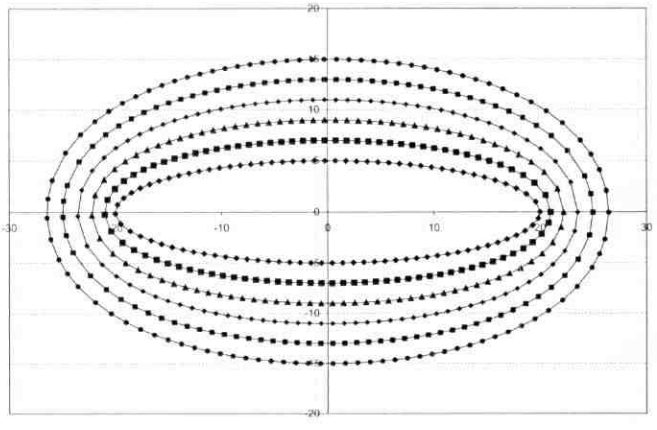

Fig. 5. Simulation of five crack growth steps from an initial 4:1 elliptical crack with an internal pressure acting normal to the crack surface. Crack growth increments are normal to the local crack front tangent and are proportional to the local stress intensity factor.

and its two neighbours. The estimated stress intensity values are compared to the analytic solution in Fig. 4. It can be seen that the agreement is excellent. (The maximum error levels were found to be less than 0.2% in this example.)

The utility of employing the stress intensity factor values to implement a simple crack growth algorithm was also tested. Fig. 5 shows the results of an incremental growth simulation where each boundary point is advanced in a direction normal to the crack front by a distance that is scaled to the local stress intensity factor. Five growth steps are shown indicating 'faster' growth in the direction of the minor axis where the stress intensity factor is the greatest.

Discussion and conclusions

The concept of extending the capability of the displacement discontinuity method to include crack edge collocation is presented in this paper. The viability of the approach is demonstrated in two simple cases for flat cracks. In these cases the enclosed crack region is convex and appropriate edge shape functions can be readily chosen. In general cases, where the crack surface geometry is more complicated (including re-entrant edge segments), it will be necessary to cover the crack surface with a suitable element tessellation. If the elements are assumed specifically to be triangular, the local edge collocation procedure appears to be entirely feasible, provided local slope continuity of the crack opening displacement function is main-

tained at element vertices. This can be achieved, for example, by determining local least squares estimates of the crack opening displacement function at each vertex or by other shape 'blending' procedures. This approach appears to offer a very useful extension to the displacement discontinuity method by providing the essential results that are required in both fracture mechanics applications and in tabular mine design procedures where the energy release rate (which can be derived from the stress intensity factor) is used to judge the extent of fracturing near the edges of the excavations.

More challenging developments of the edge collocation technique are still required to devise effective collocation schemes at crack junctions or 'kinks'. It is also of great interest to extend the method to treat problems involving curvilinear crack surfaces and to the analysis of dynamic fracture propagation processes.

I wish to acknowledge many fruitful interactions, involving both lectures and discussions with Tony Starfield. In particular, his early work in the development of displacement discontinuity boundary element methods has provided me with considerable stimulation in pursuing further applications of these methods. I would also like to thank Mark Hildyard for a number of helpful comments on the paper.

1. Salamon M.D.G. (1964). Elastic analysis of displacements and stresses induced by the mining of seam or reef deposits, Part I. *J. S. Afr. Inst. Min. Metall.* **64**, 128–149.
2. Starfield A.M. and Crouch S.L. (1973). Elastic analysis of single seam extraction. In *New Horizons in Rock Mechanics*, eds H.R. Hardy and R. Stefanko, pp. 421–439. Am. Soc. Civil Engrs, New York.
3. Crouch S.L. (1976). Solution of plane elasticity problems by the displacement discontinuity method. *Int. J. Numer. Meth. Engng* **10**, 301–343.
4. Maruyama T. (1963). On the force equivalents of dynamical elastic dislocations with reference to the earthquake mechanism. *Bull. Earthq. Res. Inst., Tokyo University* **41**, 467–486.
5. Rice J.R. (1993). Spatio-temporal complexity of slip on a fault. *J. Geophys. Res.* **98**, 9885–9907.
6. Carter B.J., Wawrzynek P.A. and Ingraffea A.R. (2000). Automated 3-D crack growth simulation. *Int. J. Numer. Meth. Engng* **47**, 229–253.
7. Crouch S.L. and Starfield A.M. (1983). *Boundary Element Methods in Solid Mechanics*. George Allen & Unwin, London.
8. Stuart A.D. (1979). *An application of the fast Fourier transform in numerical elasticity*. M.Sc. thesis, University of the Witwatersrand, Johannesburg.
9. Young A. (1996). A single-domain boundary element method for 3-D elastostatic crack analysis using continuous elements. *Int. J. Numer. Meth. Engng* **39**, 1265–1293.
10. Ryder J.A. and Napier J.A.L. (1985). Error analysis and design of a large-scale tabular mining stress analyser. In *Proc. Fifth International Conference on Numerical Methods in Geomechanics, Nagoya, Japan*, eds T. Kawamoto and Y. Ichikawa, pp. 1549–1555. Balkema, Rotterdam.
11. Vijayakumar S., Yacoub T.E. and Curran J.H. (2000). A node-centric indirect boundary element method: three-dimensional displacement discontinuities. *Computers and Structures*. **74**, 687–703.
12. Zemanian A.H. (1965). *Distribution Theory and Transform Analysis*. Dover, New York.
13. Cherepanov G.P. (1979). *Mechanics of Brittle Fracture*. McGraw-Hill, New York.

Numerical modelling of heat flow in mines

F.H. von Glehn*†, R. Hemp* and R.C. Funnell*

For deep mines with excavations situated in areas of high virgin rock temperature, most of the heat entering the excavations is via conduction through rock. The fundamental equations describing heat transfer within the rock and the transfer of this heat from the surface of the excavation to air flowing in the excavation are complex. For example, boundary conditions are not uniform and heat flow into the excavation is not symmetrical; rock surfaces may be partially wet, with convection, evaporation and radiation taking place simultaneously at the rock surface; in stopes, mining activities take place cyclically, with varying amounts of service water used at different periods in the mining cycle. Thus, numerical approximations are required to model heat flow in mines. This paper describes recent developments in the simulation of heat flow into mine excavations. In particular, models developed for underground dams and stopes are described in detail.

Introduction

To design optimum mine cooling systems that ensure a safe working environment and achieve maximum productivity combined with cost-effective operation, it is essential to be able to predict the various heat loads and cooling effects in a mine accurately.

Most of the heat entering deep mine excavations is via conduction through rock. The fundamental equations describing heat transfer within the rock and the transfer of this heat from the surface of the excavation to air flowing in the excavation are complex. For example, boundary conditions are not uniform and heat flow into the excavation is not symmetrical; rock surfaces may be partially wet, with convection, evaporation and radiation taking place simultaneously at the rock surface; in stopes, mining activities take place cyclically with varying amounts of service water used at different periods in the mining cycle. Thus, various numerical approximations have been developed. The problem has previously either been reduced to one of radial symmetry by using a uniformly damp airway to represent one that is in reality partly wet and partly dry, or a large set of partly wet cross-section problems has been solved numerically, from which a general solution based on interpolation has been developed.[1-3] These solutions have been successfully applied in software used for predicting heat loads in mines, for example, Tunnel,[4] Vuma,[5] Environ,[6] and the quasi-steady method.[7]

This paper discusses recent developments in the simulation of heat flow into mine excavations. In particular, models developed for underground stopes and dams are discussed in detail.

*Bluhm Burton Engineering, P.O. Box 786012, Sandton 2146, South Africa.
†Author for correspondence. E-mail: bbengin@global.co.za

Heat flow in underground stopes

The stoping zone is one of the principal contributors to the overall mine heat load and the use of large quantities of chilled service water is being considered to combat this heat load in deep mines. Since the 1970s, many mines have adopted chilled service water as an inexpensive means of distributing cooling, as service water is an inherent part of many mining activities. Exposed chilled service water in the working zones cools the ventilation air directly and also, as the water flows over the hot rock surfaces, it cools the rock. This cooling effect is obtained at the correct time, coinciding with the working shift, since this is the period of peak water usage.

An alternative powering system to 'conventional' compressed air, the use of hydropower (that is, high-pressure service water) has been introduced in a number of South African mines.